JOURNAL OF APPLIED PHYSICS **118**, 125308 (2015)

Semiconductor-insulator transition in VO_2 (B) thin films grown by pulsed laser deposition

Armando Rúa, Ramón D. Díaz, Sergiy Lysenko, and Félix E. Fernández[a)]
Department of Physics, University of Puerto Rico, Mayagüez, Puerto Rico 00681-9000, USA

(Received 15 June 2015; accepted 15 September 2015; published online 28 September 2015)

Thin films of B-phase VO_2 were grown by pulsed-laser deposition on glass and (100)-cut MgO substrates in a temperature range from 375 to 425 °C and at higher gas pressures than usual for this technique. The films were strongly oriented, with *ab*-planes parallel to the substrate surface. Detailed study of surface morphology through Atomic Force Microscopy images suggest significant differences in evolution as a function of growth temperature for films on the two types of substrates. Measurements of electrical conductivities through cooling-heating cycles from room temperature to 120 K showed changes of five orders of magnitude, with steeper changes between room temperature and ~150 K, which corresponds with the extended and reversible phase transition known to occur for this material. At lower temperatures conductivities exhibited Arrhenius behavior, indicating that no further structural change was occurring and that conduction is thermally activated. In this lower temperature range, conductivity of the samples can be described by the near-neighbor hopping model. No hysteresis was found between the cooling and heating braches of the cycles, which is at variance with previous results published for VO_2 (B). This apparent lack of hysteresis for thin films grown in the manner described and the large conductivity variation as a function of temperature observed for the samples suggests this material could be of interest for infrared sensing applications. © *2015 AIP Publishing LLC*.
[http://dx.doi.org/10.1063/1.4931887]

I. INTRODUCTION

Of the materials which undergo reversible metal-insulator transitions under the influence of external parameters such as temperature or pressure one of the most studied is surely VO_2,[1] which above 68 °C has a stable "metallic" phase with a tetragonal system lattice (rutile type structure, designated R) in which each V^{4+} ion is centered in a tetrahedron formed by six O^{2-} ions at the vertices. On cooling, the structure changes reversibly to a monoclinic lattice (designated M_1). This phase is non-metallic.

In addition to the M_1 and R phases, there are several other VO_2 polymorphs. One of these, designated B, has a monoclinic lattice ($a = 1.203$ nm, $b = 0.3693$ nm, $c = 0.642$ nm, $\beta = 106.6°$, and space group C2/m) and is metastable at ambient conditions.[2,3] Its structure can be described as an arrangement, parallel to the *ab* plane, of double layers (upper and lower) including slightly distorted VO_6 octahedra, which share edges of their (approximately) square base, while in the normal direction octahedra in each side of the double layer make only apical contact with those of one side of the following bilayer. Thus, the planes corresponding to these apical contacts only contain oxygen ions and the number of bonds per unit surface area is low. Hence, bonding between bilayers is weak compared to bonding within them. The layered and relatively "open" structure of this material is similar to that of V_2O_5 and V_6O_{13}, which has made all three compounds potentially interesting as electrodes for lithium-ion batteries on account of their large capacity for Li^+ intercalation.[4] Except for consideration of substrate surface structure effects, it can be expected that VO_2 (B) films will show a tendency to grow in layers with (001) crystal planes parallel to the substrate surface. This is in fact the case, although at relatively high substrate temperatures (450 °C or more) growth of other VO_2 polimorphs becomes more favorable.[5]

Upon heating, VO_2 (B) transforms to the more stable R phase at temperatures as high as 550 °C or more.[6] This is an irreversible transformation, since VO_2 (R) transforms into VO_2 (M_1) upon cooling. Thin films of VO_2 (B) have been deposited by several techniques, including sputtering and metalorganic chemical vapor deposition (MOCVD), in some cases with the explicit purpose of employing this transformation to ultimately produce VO_2 (M_1) films.[5,7] Single-phase VO_2 (B) films have been deposited on glass by MOCVD at substrate temperatures as low as 370 °C.[5] It was recently shown that VO_2(B) thin films can be lattice matched to (100)-cut $SrTiO_3$ substrates, growing them by pulsed laser deposition (PLD) at 550 °C substrate temperature.[8] Because of previous (unpublished) results in which we obtained PLD-grown VO_2 (B) films at temperatures at least 100° lower, it seemed of interest to explore the possibility of stabilizing this particular phase at these lower temperatures using PLD, even if the films were not lattice-matched to the substrate, and this was the initial motivation for the present work. Deposition on SiO_2 glass is of particular interest because it is relevant for device integration with silicon-based technology.

Once single-phase VO_2 (B) films were in fact prepared, it was decided to probe their low-temperature electrical

a)Author to whom correspondence should be addressed. Electronic mail: felix.fernandez@upr.edu

conduction characteristics, which are of interest in themselves because there are currently very few reports of these properties, and there are substantial disagreements amongst these reports. Furthermore, VO_2 (B) has a reversible transition to a lower temperature phase, first reported over two decades ago by Oka *et al.*[9] These authors performed a study of structure and magnetic properties of powder samples of VO_2 (B) in a broad temperature range and showed that, starting from near room temperature, the material undergoes a gradual transition to a different monoclinic structure (also with space group C2/m), although transformation was never complete for the sample material and the fraction of the low-temperature phase saturated at ~70% below ~150 K. According to these authors, through the transition, while the VO_2 (B) layered structure is preserved, there occur small reductions in distance between neighboring V^{4+} ions. These reductions are larger (almost a 7% reduction) for ions in the *ac*-plane, which comprise one half of the cations in the structure.

This pairing of the V^{4+} ions could be expected, as originally proposed in the case of the VO_2 R → M_1 transition,[10–15] to cause a diminution in the material's electrical conductivity as the temperature is lowered. However, since the phase transition of VO_2 (B)occurs gradually over a very broad temperature range of ~150 degrees, unlike in the VO_2 (R) → VO_2 (M_1) case, the associated conductivity change in VO_2 (B) cannot be expected to be sharp. In fact, electrical measurements of resistivity at low temperatures first reported for B-phase (i.e., when at room temperature) VO_2 pressed powder pellets showed a conductivity drop by more than three orders of magnitude as the sample was cooled from room temperature, with initial value of ~1 S/m, to nearly 2×10^{-4} S/m by 160 K.[16] These results also evidenced hysteresis between cooling and heating, although no full cycles were presented and the large discrepancy between resistivity values upon cooling and heating at the lowest temperature range measured was not explained. Resistivity measurements over a range from 400 K to 150 K were reported very recently for VO_2 (B) films grown by PLD on (100) $SrTiO_3$ substrates at 500 °C.[17] In this latter case, in which the resulting films were epitaxial with the substrate, a conductivity drop by 4 orders of magnitude (from $\sim 5 \times 10^4$ S/m at 400 K to ~5 S/m at 150 K) was found, with nearly full heating-cooling cycles showing hysteresis loops with a breadth of over ~15 K and maximum rate of change near 200 K. While the two reports in which electrical properties of VO_2 (B) were measured at below-ambient temperatures evidenced a large reduction in conductivity as the temperature was lowered, the details differ greatly, no doubt in part because the two types of samples used were very different in nature. Hence, it seemed of interest to further explore the conductivity of VO_2 (B) films as a function of temperature. As described later (Section III C), some of the electrical characteristics found for the resulting films were unexpected.

For the present work, the background gas used for PLD was a mixture of argon and molecular oxygen. Using this mix instead of pure O_2 offers an additional control parameter so that buffering of the high kinetic energy species and oxidation are partially decoupled. In PLD both of these functions are usually performed by the same reactive gas, O_2 in the case of oxide film growth. Buffering is indispensable in PLD because of the very high speeds at which particles are emitted from the target. In fact the plume formed when a target is ablated in a background gas can be "split" in two components, one of which consists of particles which continue to travel at speeds close to those which obtain right after ablation (~10^4 m/s or more), while the other includes particles which are substantially slowed.[18] The fast component can even cause "re-sputtering" of the deposited material in some cases,[19] but impingement of species with moderately high kinetic energies (tens of eV) enhances adatom mobility on the surface of the growing films and can promote crystallization even at low substrate temperatures in comparison with most other vapor deposition techniques. The range of gas pressures of interest for PLD, assuming common parameters for laser fluence (several times the threshold fluence for the target and laser wavelength used) and target-substrate distance (4 to 7 cm) usually extends from ~5 to ~75 mTorr. At higher pressures, species impinging on the substrate are mostly thermalized and adatom mobility would depend mainly on substrate temperature. The film growth process would be closer then to that obtained with "thermal" techniques such as evaporation. At even higher background pressures (over ~150 mTorr), the speeds of the ablated species become low enough that nanoclusters can be formed in the expanding shock wave initially produced by the interaction of the ablated material and the background gas.[20]

Since the target used for film growth in the work reported here was not a vanadium oxide but metallic vanadium, most of the oxygen incorporated onto the film is necessarily provided directly from the chamber atmosphere, except for a likely small amount from a thin oxide layer formed on the target itself as ablation proceeds over the same track on the rotating target. Atomic oxygen and other oxygen radicals, which are much more reactive than molecular oxygen, are produced by dissociation or excitation of O_2 molecules in the gas via collisions with species ejected from the target with high kinetic energies and directly by the laser beam (photodissociation) in the high fluence region near the target surface. These oxygen radicals can react with vanadium in the gas phase or with the material already deposited on the substrate. In-between pulses, and after deposition is completed and the sample is cooling down, reactions between the film surface and molecular oxygen will also occur, although oxidation is then much less significant. On the other hand, while the substrate remains heated, rearrangement and evolution of the deposited species is favored, which promotes crystallization and grain growth.

In the past, we have been able to grow high quality VO_2 (M_1) thin films using an O_2 - Ar mixture as background gas.[21] For the present work, attempting to grow VO_2 (B) films at lower temperatures, the total pressure used was high enough that the particle speeds were expected to have been substantially moderated, and this should favor oxidation of the vanadium vapor in transit to the substrate. On the other hand, while formation of small vanadium oxide clusters before reaching the substrate is possible, the total pressure was not high enough to expect large numbers of them.

A recent study of plume dynamics during PLD growth of VO_2 thin films on glass substrates (at 500 °C) indicated that phase purity and vertical grain sizes (~40 nm) of the resulting M_1-phase films were optimized at a background gas (pure O_2) pressure of ~7.5 mTorr and that both purity and grain size were rapidly degraded at higher pressures.[22] As shown in the following, it turns out that the situation is very different at least in the case of VO_2 (B) film growth, since excellent quality films, with large vertical grain sizes (~70 nm, comparable to film thickness) were obtained on glass substrates through a growth procedure which included total background gas pressure almost one order of magnitude higher and growth temperatures as low as 375 °C. As in this case, it seems clear one cannot assume that experience with preparation of one VO_2 phase can be readily applied to a different one.

II. SAMPLE PREPARATION

For the work described here, VO_2 film samples were grown by PLD on different substrates (SiO_2 glass, (100)-cut MgO, and (100)-cut $SrTiO_3$). Deposition was performed by ablating a vanadium metal target in an oxygen and argon atmosphere, at a total pressure of 70 mTorr, measured with a diaphragm capacitance sensor. Gas flows of 10 standard cm^3/min (sccm) Ar and 15 sccm O_2 were independently adjusted with mass flow controllers.

The growth temperatures found to produce pure or nearly pure B-phase VO_2 were in the range from 375 to 425 °C for both glass and MgO substrates. At substrate temperatures outside this range x-ray diffraction (XRD) analysis showed very clear peaks from other vanadium oxide phases. Samples on glass and MgO substrates were grown simultaneously for each temperature, while those on $SrTiO_3$ were grown in separate runs under nominally identical conditions. It was not possible to grow samples of adequate size on all three types of substrate simultaneously because of the relatively small area for adequate thickness uniformity in our PLD system.

Substrates were cleaned prior to film growth by sequential ultrasonic baths in trichloroethylene, acetone and methanol and were attached to the deposition vacuum chamber's substrate heater. The crystal substrates, which had polished surfaces, were not etched or treated in any particular manner before film growth, aside from chemical cleaning. For all depositions, the vanadium target was ablated by KrF excimer laser pulses at a fluence of ~4 J/cm^2 and a frequency of 10 pulses per second. The distance between target and substrate was 4 cm. Background pressure before depositions was ~10^{-6} Torr before the heater temperature was increased, Ar and O_2 gas flows were started, and the pump was throttled to increase the pressure to 70 mTorr. Deposition time was 10 min for all samples. After film growth, the heater was turned off, gas flows were stopped, and samples were allowed to cool in vacuum. No post-deposition heat treatment was performed. Sample thicknesses were subsequently measured with a stylus profilometer, using a step created on the sample by masking part of the substrate before deposition. Except as noted, all samples were ~100 nm thick, which means that the average growth rate was ~0.17 nm/s. From the resulting film structural orientation, which is discussed in Section III, and the known lattice parameters, the relevant monolayer spacing is 0.61 nm, so this growth rate cannot be considered very large. B-phase VO_2 films had a characteristic deep purple color as seen on reflection.

III. RESULTS AND DISCUSSION

A. Crystal structure

Crystal structure for each sample was determined by XRD performed with CuK_α radiation in a Bruker-AXS D8 Discover diffractometer with parallel-beam geometry and using a θ-2θ configuration. All samples deposited on glass and MgO under the conditions described evidenced strong preferential out-of-plane orientation, with VO_2 (B) *ab*-planes parallel to the substrate surface. This is consistent with the layer structure of the material, as discussed in Section I. For samples grown on (100)-$SrTiO_3$ within the same range of conditions as for the other two types of substrate, it was never possible to obtain pure or nearly pure B-phase VO_2. In fact, substrate temperatures of 550 °C or more had to be used to obtain VO_2/$SrTiO_3$ films which included the B phase, but even in those cases strong diffraction peaks corresponding to either the A phase or the M_1 phase, or both, were found. Since the intention of the study reported here centers on pure or nearly pure B-phase VO_2 films stabilized at lower temperatures, no further results are included in the following for the films grown on $SrTiO_3$.

For samples grown on SiO_2 glass substrates strong (00*l*) reflections for VO_2 (B) were observed, with *l* at least up to third order. Fourth and fifth order (00*l*) reflections, which have much lower intensities,[23] were observed for the samples grown at lower temperatures. Compared with reference powder diffraction reflections, all (00*l*) peaks for samples on glass where shifted to higher angles, more so for higher order reflections, indicating tensile strain in the films. Figure 1 shows the XRD result for the VO_2/glass sample grown at the highest temperature (425 °C). Besides the VO_2 (B) (00*l*) peaks, there is a weak peak attributed to the strongest reflection for the VO_2 M_1 phase. Thus, a small admixture of this

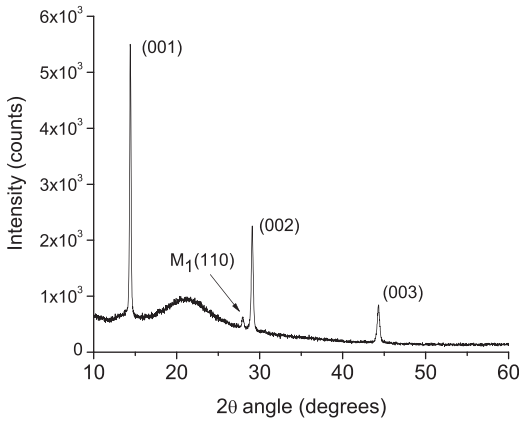

FIG. 1. X-ray diffraction scan for VO_2 sample deposited on glass at 425 °C. Main reflections correspond to the B phase.

phase, usually obtained in samples deposited by PLD at higher temperatures and lower oxygen pressures is present in the sample. The broad peak near $2\theta = 21°$ is caused by the glass substrate. For the samples grown at the lower temperatures on glass, in addition to the strong (00*l*) peaks, several very low-intensity peaks were observed, some of which are attributable to VO_2 (B) (200) and (400) reflections, suggesting that although the (001) orientation is clearly favored, some out-of-plane disorder remains.

For samples grown on (100)-cut MgO substrates XRD results again show strong VO_2 (B) (00*l*) reflections with *l* up to the fourth order, as shown in Fig. 2, for a sample grown at 400 °C. This sample appears to be nearly-pure B-phase. However, the sample deposited at 425 °C on MgO resulted in a mix of A and B phases, as shown by clear A-phase (*hh*0) reflections up to third order,[24] in addition to the B-phase (00*l*) reflections, along with several very small peaks which could not be unambiguously attributed. Production of the A phase is not surprising, since at even higher growth temperatures it can be produced at relatively high O_2 pressures and laser pulse rates.[17] Nevertheless, it is noted that XRD scans for the sample grown on glass simultaneously with this sample on MgO did not reveal any A-phase peaks. This underscores the importance of the substrate in stabilizing the resulting VO_2 phase.

The (00*l*) B-phase peaks for the VO_2/MgO sample grown at 400 °C are slightly shifted to lower angles, indicating that, contrary to the samples deposited on SiO_2 glass, the film is in compression. This is attributed to the large differences in thermal expansion coefficients of fused silica glass and MgO, with values of $0.5 \times 10^{-6}\ K^{-1}$ and $13.5 \times 10^{-6}\ K^{-1}$, respectively.[25] While thermal expansion coefficient values for R-phase and M_1-phase VO_2 (which change substantially through the structural transition) have been published decades ago,[26] we are not aware of similar data for B-phase VO_2. Considering the observed shifts of the XRD peaks, it is suggested that the thermal expansion coefficient of B-phase VO_2, at least on average along the *ab*-plane, has a value intermediate between those of fused silica glass and MgO, but closer to the latter, which in turn would place it closer to the average value for R-phase VO_2 ($13.35 \times 10^{-6}\ K^{-1}$). From the widths of the (00*l*) XRD peaks for samples grown on either glass or MgO, after correcting for instrumental broadening, crystallite sizes along the substrate normal were estimated using the Scherrer equation. Values of ~70 nm were obtained in all cases, which is consistent with sample thicknesses.

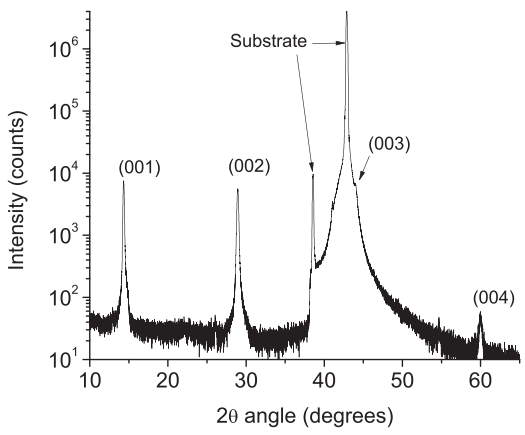

FIG. 2. X-ray diffraction scan for VO_2 sample deposited on (100)-MgO at 400 °C. Reflections for VO_2 (B) are labeled. Substrate peaks correspond to MgO (200) reflections for CuK_α and CuK_β radiation.

Clearly, lattice matching with the substrate is an important factor favoring VO_2 (B) growth for films grown on $SrTiO_3$ at higher temperatures and lower oxygen pressures. The interesting epitaxial relationship between VO_2 (B) and (100)-$SrTiO_3$ has been described by Chen *et al.*,[8] and relies on the fact that this cubic crystal has a lattice size $a = 0.3905$ nm, which is approximately one third the length of the VO_2 (B)*a* lattice size and approximately equal to its *b* lattice size. Thus, it can accommodate with relatively low strain the VO_2 (B) (001) crystal surface. Other cubic crystals with lattice constants similar to $SrTiO_3$ may serve as epitaxial templates for VO_2 (B) as well. In contrast, MgO has a lattice size $a = 0.4212$ nm, which is too far from being a submultiple of the VO_2 (B) *a* and *b* lattice parameters. This severe mismatch will impede epitaxial growth. It is an open question why, with the growth conditions employed in the present work, VO_2 (B) preferentially stabilizes on MgO substrates, on which epitaxial growth is not favored, and on glass, on which it is impossible, but only in a very limited manner on (100)-$SrTiO_3$.

B. Surface morphology

The surfaces of the samples were studied by atomic force microscopy (AFM) in contact mode using a Park Scientific Autoprobe CP instrument. Figure 3 shows 1 μm × 1 μm AFM images and analysis results of the VO_2/glass samples. It is emphasized that the study presented for the images is an analysis of the surface roughness, which uses information from the 256 × 256 pixels available, not a statistical study of grain sizes, although average lateral grain sizes have been also estimated by direct measurements on the images. Raising the growth temperature from 375 °C to 425 °C has resulted in a gradual increase of the lateral grain sizes and sample roughening. The average surface grain size *d* increases from ~50 nm to ~90 nm, the latter number being comparable to film thickness. The histogram of the surface height distribution (SHD) (Fig. 3(b)) broadens and becomes more asymmetric, an indication of greater differences between valleys and peaks, which may be also noticed by inspecting the images and their corresponding depth scales, shown under each AFM image in the figure. The full width at half maximum (FWHM) of the SHD increases from 2.3 to 5.3 nm: this correlates with the root-mean-square roughness (δ_{rms}) values of the samples, which increase from 2.6 nm to 3.9 nm (see inset in Fig. 3(b)). Comparison of the profiles along a diagonal for each of the AFM images (see inset in Fig. 3(c)) indeed shows an increasingly rough aspect with higher growth temperature. Such temperature dependence of the surface morphology is expected for thin films synthesized on amorphous substrates. The growth of larger grains occurs due to increased mass transfer rate in lateral

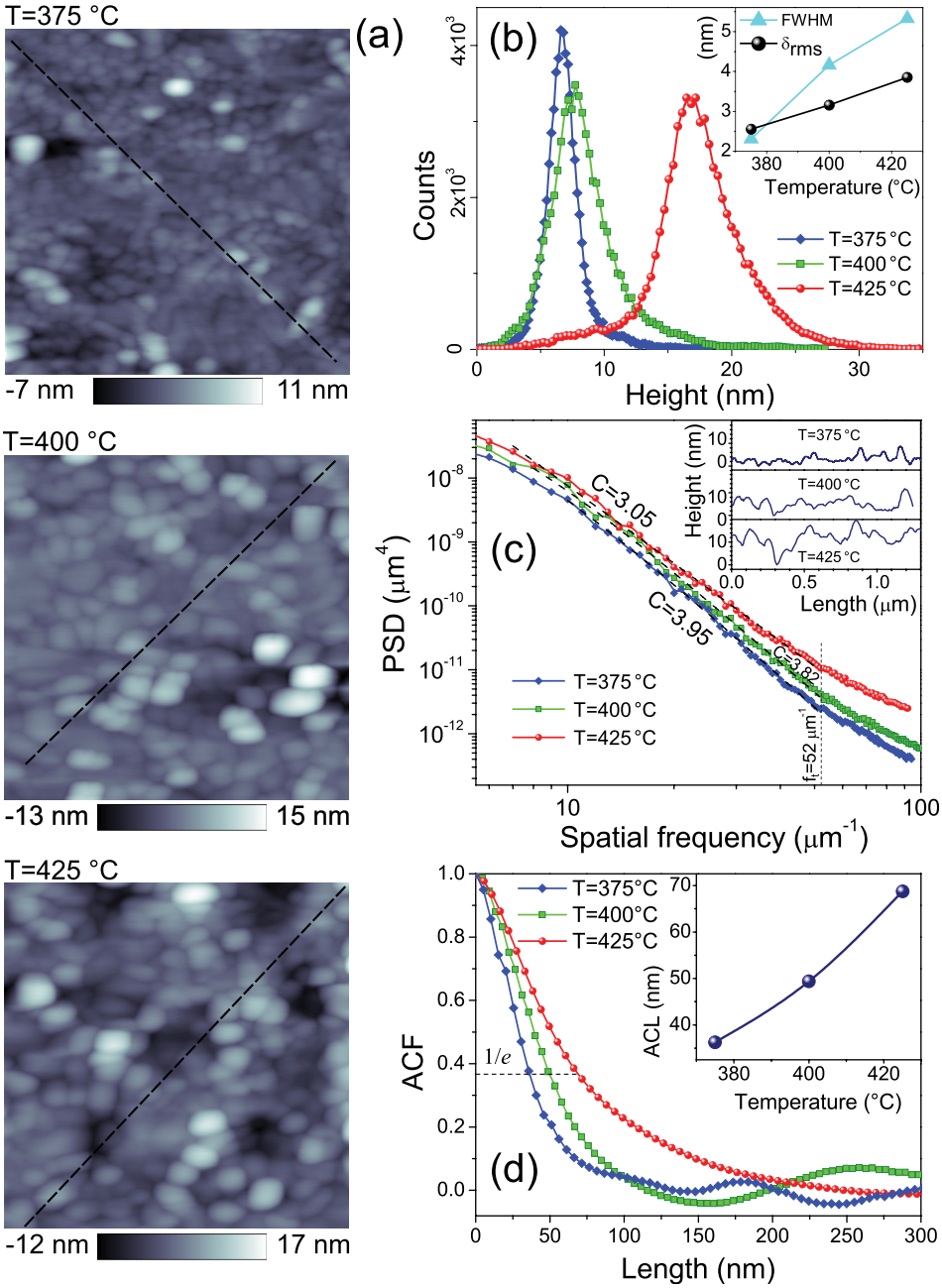

FIG. 3. (a) AFM images (1 μm × 1 μm scans) for VO_2 samples grown on glass at the indicated temperatures. (b) Surface height distributions for the three samples at left; inset: FWHM for the distributions and *rms* roughness δ, as a function of sample growth temperature. (c) PSD functions for the three surfaces; inset: surface profile for each sample, taken along the diagonal indicated by dashed lines in the corresponding AFM image in (a). (d) ACF for each sample at left; inset: autocorrelation length as a function of growth temperature for the samples.

directions at higher deposition temperatures. Recalling that crystallite sizes estimated from Bragg peak widths (~70 nm) are similar to sample thicknesses (~100 nm or less) the lateral size and shape of the structures suggests these are domes of columnar structures originating from island growth after nucleation. Because the lateral grain sizes are generally not greater than sample thickness, it appears that at the growth temperatures employed normal (three-dimensional) grain growth has not saturated.[27]

Although AFM images of the samples grown on (100)-cut MgO crystals (see Figure 4(a)) appear at first sight to be very similar to those grown on glass, closer analysis reveals very significant differences, and in fact some of their resulting morphological characteristics as growth temperature was increased from 375 °C to 425 °C change in opposite ways to those of the VO_2/glass samples. With increasing growth temperature the sample's surface height distribution (Fig. 4(b)) narrows from 3.0 to 1.9 nm and the δ_{rms} value gradually decreases from 2.9 nm to 1.6 nm (see inset in Fig. 4(b)). Comparison of the profiles along a diagonal for each of the AFM images (see inset in Fig. 4(c)) shows a much more flattened aspect for the sample grown at the highest temperature: again the opposite of the case for the samples on glass. Measurements taken directly on these AFM images show the presence of two sets of grains with different characteristic sizes. The average lateral size of the smaller grains (~75 nm) is nearly independent of growth temperature, while for the larger grains their average size decreases from ~130 nm at 375 °C to ~100 nm at 425 °C. Also, it is noticed that the surface height histogram in Fig. 4(b) for these samples can be approximated as a sum of two normal (Gaussian) distributions, one of which is centered at 9.1 nm, independently of growth temperature, while becoming shallower with increasing temperatures. Hence, this distribution correlates with the

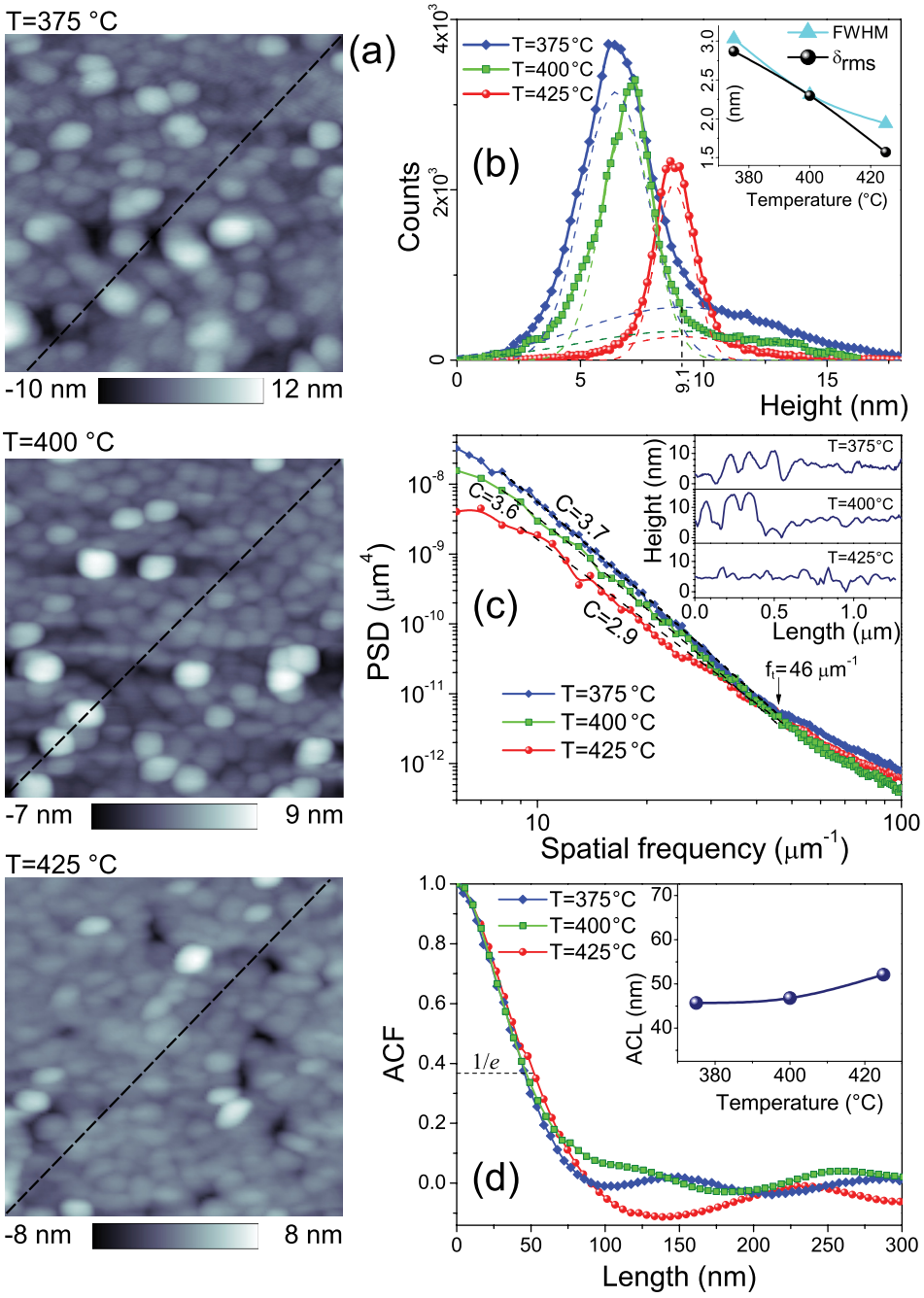

FIG. 4. (a) AFM images (1 μm × 1 μm scans) for VO_2 samples grown on (100)-MgO at the indicated temperatures. (b) Surface height distributions for the three samples at left; inset: FWHM for the distributions and *rms* roughness δ, as a function of sample growth temperature. (c) PSD functions for the three surfaces; inset: surface profile for each sample, taken along diagonal indicated by dashed lines in the corresponding AFM image in (a). (d) ACF for each sample at left; inset: autocorrelation length as a function of growth temperature for the samples.

group of larger grains. At the highest growth temperature (425 °C), the difference between the two groups is much reduced, the position of the two normal distributions almost coincides and, in consequence, the height distribution is not just sharper but nearly symmetric.

Additional information about surface morphology was obtained from the analysis of the power-spectral-density (PSD) and autocorrelation function (ACF) of the surfaces.[28] The PSD function is related to the "roughness spectrum" and, for isotropic roughness

$$\delta_{rms}^2 = 2\pi \int PSD(f) f df, \tag{1}$$

where f is the spatial frequency of the surface. The ACF is the height-height correlation function of the image with itself, and is the Fourier transform of the PSD. The PSD functions obtained from AFM scans can be described by a two-dimensional "ABC" mathematical model given as

$$PSD = \frac{A}{\left[1 + (Bf)^2\right]^{(C+1)/2}}, \tag{2}$$

where A, B, and C are constants.[29] Constant A is the PSD value for the low spatial frequency limit, while B is the inverse of a "drop-off" frequency after which the PSD falls more rapidly and which depends on the correlation length of the surface. Constant C defines the power-law exponent which models the steepness of this drop for higher frequencies. This last constant, which can be extracted from the slope of the PSD function in a log-log graph, is the most

informative parameter which can be derived from modeling experimental PSD data by Eq. (2). As shown in Figs. 3(c) and 4(c), the PSD function for each film has three distinct regions. The lowest spatial frequencies, under $\sim 10\ \mu m^{-1}$ ($d \geq 100$ nm), which are only partially shown in the graphs, correspond to irregularities with relatively large dimensions (along the sample plane). These include contributions from substrate surface waviness or scratches, because the thin film will replicate these larger features. The intermediate region, from $f \sim 10\,\mu m^{-1}$ up to a certain threshold frequency f_t, has nearly constant (and relatively steep) slope for each film; this mostly contains the roughness contributions of the grains themselves. Above f_t, which has values of $52\,\mu m^{-1}$ ($d \leq 19$ nm) for the VO_2/SiO_2 films and $46\,\mu m^{-1}$ ($d \leq 22$ nm) for the VO_2/MgO films, the parameter C is reduced by a factor of ~ 2. Irregularities with a flatter roughness spectrum at these very high spatial frequencies are believed to correspond mainly to regions between grains.

From Fig. 3(c), it can be noticed that PSD values are higher for the VO_2/glass samples grown at higher temperatures. This is consistent with the idea that roughening has increased with growth temperature. Contrarily, as seen in Fig. 4(c), PSD values are lower for the VO_2/MgO samples grown at higher temperatures. However, in both cases, the PSD slope is steeper (higher C value) for samples grown at lower temperatures. The straight portions of the graphs are indicated by dashed lines in Figs. 3(c) and 4(c), and the C values for the model in each case are shown next to the lines. Figures 3(d) and 4(d) show the surface ACF for the two groups of samples and, as an inset in each figure, the autocorrelation length (ACL) for each sample, defined here as the half-width of the ACF at $1/e$ of the zero-lag (or zero-length) value. For the samples grown on glass, the ACL increases substantially with growth temperature, from 36 nm to 69 nm, and the ACF tail is also much longer for the sample grown at the highest temperature, evidencing the increasing lateral coherence. In comparison, for the samples deposited on MgO, there is only a slight increase in ACL with growth temperature (from 46 nm to 52 nm), and the ACF tails are all short in comparison, crossing zero at a lag length of ~ 90 nm for two of the cases. These results for the samples on MgO lend support to the previous remarks about the two groups of grains observed in these AFM images.

As to the possible origin of the differences revealed by AFM analysis of the samples grown on either glass or (100)-MgO, we believe these are caused mainly by differences in nucleation and growth at the early stages. Aside from the surface structural differences (which would be limited to some extent by the fact that the MgO substrates were not etched before film deposition), it is appropriate in a first approach to consider the surface energy densities (per unit area) of the different surfaces involved. Recalling the concepts of capillarity theory, one defines the spreading parameter S[30]

$$S = \gamma_s - (\gamma_f + \gamma_{sf}), \tag{3}$$

where the γ terms are, respectively, the surface energies per unit area for the substrate (s), the film material (f) and the substrate-film interface (sf). For positive S, if the film material is a liquid, it will tend to spread completely over the substrate, since that will lower the surface energy of the system. For negative S the film material will tend to agglomerate and not wet the substrate completely. These concepts can be applied to the case of thin solid film growth when the temperature is high enough that mobility of surface atoms is enhanced, as is often the case during vapor deposition or post-deposition annealing.

The reported surface energy density of SiO_2 glass is $\sim 0.3\ J/m^2$ and is not expected to vary greatly between room temperature and the growth temperatures of interest here.[31] This is much less than the measured values for (100)-MgO surfaces ($\sim 1.2\ J/m^2$).[32] The surface energy densities for low-index surfaces of VO_2 (B) have been calculated,[33] and the results given for the (001) surfaces are $0.49\ J/m^2$ and $0.38\ J/m^2$ for unrelaxed and relaxed surface atoms, respectively. Hence, without including the effect of the relevant interfacial film-substrate energy densities (γ_{sf}), which to our knowledge are not available in the literature, substrate coverage appears to be energetically more favorable for (100)-MgO than for glass. However, in neither case the condition $S > 0$ in Eq. (3) would be satisfied, so film growth is expected to proceed by means of island nucleation and growth (Volmer–Weber mode),[34] even though the crystal structure of the film grains is layered, as shown by the XRD results. The measured *rms* roughness values for the films grown at 375 °C on glass and MgO were very similar (2.6 and 2.9 nm, respectively), but developed in stark contrast for higher growth temperatures, increasing to 3.9 nm for the sample on glass and diminishing to 1.6 nm for the sample on MgO for the samples grown at 425 °C. Thus, for the higher growth temperatures, a larger value (less negative) of the spreading parameter S seems in agreement with the lower surface roughness. The reduced kinetics of adatoms at the lowest growth temperature may help explain why in that case there is little difference in roughness values for the films on the two substrates. Lower values (more negative) of S can indicate a tendency to "dewetting" or agglomeration of the growing film, causing formation or growth of holes and even delamination of the film.[35] In the AFM images for the VO_2(B) samples grown on both types of substrates at the highest temperature, a few depressions can be observed (see Figs. 3(a) and 4(a)) which could correspond to small holes (smaller than grain sizes), although the AFM scans are not sufficient to verify if these are indeed holes. In any case, no instances of large holes or edge retraction were observed in the AFM scans for any of the samples. This suggests that the film-substrate interface energy density values (γ_{sf}) are low for VO_2(B) on either type of substrate.

The preceding remarks rely on simple ideas of capillarity theory. A deeper treatment would require consideration of surface stresses and in-plane crystal structure,[34,36] as well as application of additional characterization techniques, and is beyond the scope of the present work. Finally, it is noted that the measured average surface energy density of the $SrTiO_3$ (100) surface has been reported as $\sim 2.85\ J/m^2$.[37] Therefore, coverage of this surface by (001)-oriented VO_2 (B) can seem even more favorable energetically than for

(100)-MgO, even without considering the demonstrated lattice match. However, under the range of growth conditions employed in the present study competition with other VO_2 phases (particularly the A phase) impeded stabilization of the B phase exclusively or even primarily.

C. Conductivity as a function of temperature

Conductivity (σ) measurements were performed in a 4-point van der Pauw configuration. The samples were attached to a sapphire wafer in the cold finger of a closed-cycle helium refrigerator and gold wires were bonded to the corners of the rectangular samples. The temperature was ranged from ambient to as low as it was still possible to make electrical measurements accurately for specific samples, which was limited to an upper resistance value of ~10 GΩ. For all samples, full heating-cooling cycles were completed. The heating and cooling ramps used were 2 K/min and, in order to minimize the effect of delays between the sensed temperature and the actual sample temperature, the measuring program included a waiting time of 2 min once each preset temperature was reached. Samples were in the dark through all resistance measurements. As usual, measurements were taken by injecting current between each pair of consecutive contacts and measuring voltage between the other two, including polarity reversals, and correcting for sample asymmetry. Average sheet resistances at each temperature were determined and the bulk sample conductivity was calculated using the measured sample thickness.

Figure 5 shows an Arrhenius-type plot of the electrical conductivity for two of the samples, measured in the range from room temperature to 120 K. Over this range, conductivities changed by five orders of magnitude. The relatively rapid change in conductivities from room temperature to ~150 K corresponds to the gradual and incomplete phase transition first reported for VO_2 (B) by Oka *et al.*[9] It is noted particularly that no hysteresis was detected between the cooling and heating parts of the cycles: the cooling and heating curves essentially overlap almost exactly over the full temperature range. Consideration of instrumental errors in the measurements, particularly in the region of steepest descent, indicates that hysteresis cannot be larger than 0.3 K, if present at all. The same lack of measureable hysteresis was found for all samples deposited under the conditions reported in this work. For temperatures under ~150 K, the graphs exhibited Arrhenius behavior, confirming that no further structural change is occurring.

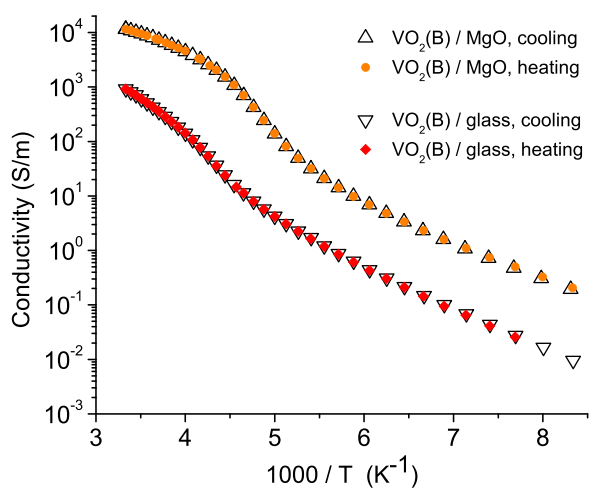

FIG. 5. Conductivity (log scale) vs. inverse temperature for samples deposited on glass at 425 °C (lower curves) and for sample deposited on (100) MgO at 400 °C (upper curves). Measured curves for cooling and heating overlap in both cases, as shown.

The lower curve in Fig. 5 corresponds to the sample grown on glass at 425 °C (80 nm thickness). Conductivity drops rapidly as soon as cooling starts, attaining its steepest descent by ~230 K and then falling less rapidly until ~150 K; afterwards, it falls linearly in the Arrhenius plot. For the samples grown on glass at the two other temperatures, the conductivity curves (not shown in the figure) are nearly identical in shape, including the lack of measurable hysteresis. The main difference is a vertical shift, which is small between curves for the samples grown at 400 °C and 425 °C (with a conductivity difference of less than 5% through most of the range), but more significant for the sample grown at 375 °C, with conductivity values over 60% higher than for the case shown. The lower conductivity of the VO_2 (B)/glass samples grown at higher temperatures may be associated with the roughening observed through the AFM analysis.

The upper curve in Fig. 5 shows results for the VO_2 (B)/MgO sample grown at 400 °C. The curve is very similar to that for the sample on glass, but conductivity values are over one order of magnitude higher though the complete temperature range. As the temperature is lowered through the transition, the curve is initially slightly less steep, but has a more pronounced shoulder near 225 K, and its slope is again slightly smaller in the linear portion for temperatures under ~150 K. The samples grown on MgO at other temperatures showed similar conduction behavior but substantially lower values (about 70% lower conductivities for most of the range), which are attributed, at least in part, to the presence of other phases, particularly the VO_2 (A) phase for the sample grown at 425 °C, which was found to be present from the XRD results.

Compared with the values measured by Srivastava *et al.* for their epitaxial VO_2 (B)/$SrTiO_3$ films,[17] conductivities for the samples grown on MgO are lower by approximately a factor of two throughout the overlapping temperature range (those authors measured in the range from 400 K to 150 K and we measured from 300 K to 120 K or lower, depending on the sample). Lower conductivities are expected in the present case because the films are polycrystalline and in-plane ordering should be either very poor (for samples on MgO) or nonexistent (for samples on glass). This disorder and the limited size of crystallites will reduce electrical conductivity with respect to bulk crystal values mainly through grain boundary (GB) defects. These can trap carriers and cause depleted regions near them. Charges immobilized in trapping centers present potential energy barriers which must be overcome by mobile carriers in order to transfer between crystallites when an external electric field is applied.[38] If resistance to carrier flow is much lower through the interior of

crystallites than through GB defects, then the latter will dominate conductivity values for the film.

Since the material undergoes a phase transition through most of the measured temperature range, an analysis of the relevant conduction mechanisms would be complicated and require much more experimental information than the $\sigma(T)$ results offered here. However, for the $T \lesssim 150\,K$ range in which we were able to measure conductivities all *log* (σ) *vs.* 1/T curves are linear, revealing that conduction is dominated by a thermally activated process. These low-temperature linear portions may be described according to models which depict carrier transfer through GB defects in disordered materials. Recalling the AFM scans, we note that crystallites (inside which conduction is expected to be bulk-like) in the samples are fairly large in comparison with the boundaries. Under these conditions, one may expect the nearest neighbor hopping (NNH) model to be applicable, although we also considered Mott's variable range hopping (VRH) model.[39,40] The NNH model assumes that carrier transfer ("hopping") is most likely to occur between nearest neighbor sites and that the activation energy between these sites is constant. This model leads to a pure Arrhenius σ(T) dependence

$$\sigma_{NN} = \sigma_O \exp\,[-(E_a/kT)], \tag{4}$$

where E_a is the activation energy and σ_o is a factor independent of T. In contrast, the VRH model recognizes that at sufficiently low temperatures in disordered systems hopping between nearest neighbor sites can be less probable than between more distant sites with energy levels close to the Fermi level. This model leads to a slower temperature dependency for the conductivity in which the exponential term is a function of $T^{-1/4}$ instead of T^{-1} and the pre-exponential term includes a $T^{-1/2}$ factor. Fitting of experimental data to the VRH model allows estimation of the density of localized states near the Fermi level $N(E_F)$ and the decay constant α of the wave function for these states.[41] However, application of this model in the present case yields physically unrealistic results for $N(E_F)$ and α (over $10^{72}\,cm^{-3}\,eV^{-1}$ and over $10^{25}\,cm^{-1}$, respectively) and it was concluded that it is not suitable.

Application of the NNH model in the low-temperature region produced very good fits to the data and the values obtained for the activation energy E_a and pre-exponential factor σ_o for the different samples are presented in Table I. No results are presented for the sample grown on glass at 400 °C because its high sheet resistance impeded measurements at temperatures below 150 K.

TABLE I. Results of NNH model fits (T < 150 K).

Substrate	T_{growth} (°C)	E_a (meV)	σ_o (S/cm)
MgO	375	122 ± 2	240 ± 40
MgO	400	111 ± 2	100 ± 20
MgO	425	119 ± 1	51 ± 5
Glass	375	139 ± 3	110 ± 20
Glass	400	…	…
Glass	425	141 ± 1	83 ± 3

The activation energies determined are much higher than the thermal energies in the range ($kT \lesssim 13\,meV$) so the probabilities for surmounting the GB barriers are very low and hence conductivities under low applied fields are very low as well. The values of the activation energies are very similar for samples grown on the same type of substrate, independently of growth temperature, but are ~20 meV higher for the samples grown on glass. Thus, the lower conductivities measured for the latter can be related to higher potential barriers caused by greater in-plane disorder. On the other hand, the pre-exponential factor σ_o shows a clear tendency to higher values for lower sample growth temperatures, particularly for the samples on MgO. This behavior may be related to the possible appearance of small holes in the films at higher growth temperature, as was mentioned in Section III B, but the effect seems too strong for this to be its single cause.

The highest conductivities measured at room temperature for the VO_2 (B)/MgO samples were $\sim 10^4$ S/m, which is lower than for VO_2 (M_1) in its "metallic" phase, but still as high as for the most conductive semiconductors. Higher values are possible for epitaxially grown films, as already shown by Srivastava *et al.*,[17] or by suitable doping. The effects of the latter have yet to be studied in this material.

The most remarkable difference found with respect to the few published studies of electrical conduction for VO_2 (B) is the lack of detectable hysteresis observed in the present work for all samples grown on either glass or MgO substrates. This was repeatedly observed for all samples produced within the range of growth conditions described here. It is possible that the high defect density in the films reduces the energy barrier for the phase transformation. The "extended" and gradual nature of the transition between VO_2 (B) and the low-temperature phase already suggests that transformation energy must be distributed in some fashion over a very large temperature range (~150 K). It should be interesting to perform calorimetric measurements on this material over that temperature range, as well as to further study electrical properties of VO_2 (B) thin films with different microstructural characteristics. However, the lack of hysteresis observed in the present case, along with the demonstrated five order of magnitude change in conductivities between room temperature and ~120 K, suggests the material as a candidate for sensing applications. Naturally, the fact that employing this full temperature range would require cooling the device impedes utilization in uncooled detectors. Nevertheless, it is noted that in the range from 300 K to ~250 K, which for a microdevice can be easily reached using thermoelectric cooling, the resistance changes sufficiently rapidly, particularly for the VO_2 (B)/SiO_2 glass samples, as to warrant some interest. The temperature coefficient of resistance (TCR) in this range, calculated from the σ(T) measurements for these samples on glass was $-3.6\%\ K^{-1}$. For temperatures very close to room temperature TCR is reduced to $-2.75\%\ K^{-1}$, which is still an attractive value. While we did not perform conductivity measurements at temperatures higher than 300 K in this work, the tendency of the log(σ) *vs.* 1/T curves (Fig. 5) and the fact that the phase transition to VO_2 (B) is already completed at room temperature suggest

that the TCR value will not be reduced appreciably at temperatures at least somewhat higher than this.

IV. CONCLUSIONS

Nearly pure B-phase VO_2 thin films were grown by PLD on SiO_2 glass and (100)-MgO using lower temperatures ($\sim$100 K lower at least) and higher O_2 pressures (almost an order of magnitude more) than previously reported for PLD growth of this metastable VO_2 phase on (100)-$SrTiO_3$. Samples grown on this last substrate under the present conditions always resulted in mixed VO_2 phases. Samples on the first two types of substrates were strongly oriented with VO_2 (B) *ab*-planes parallel to the substrate surfaces. Subtle but significant differences in surface morphology were found through analysis of AFM images of the films deposited simultaneously on glass and MgO substrates, which suggests that the early stages of nucleation and film formation of VO_2 on different substrates should be further studied. Electrical conductivities at lower temperatures were modeled according to the nearest-neighbor hopping model and activation energies of $\sim$120 meV and $\sim$140 meV were determined, respectively, for samples grown on MgO and on glass. With conductivities ranging from $\sim 10^4$ S/m at room temperature to $\sim 10^{-1}$ S/m at $\sim$120 K for the samples on MgO (and one order of magnitude less for the samples on glass), the VO_2 (B) films produced have electrical properties which can make them useful for low-temperature or infrared sensing applications. Thin VO_2 (B) films grown on SiO_2 glass at temperatures as low as 375 °C and without further heat processing can be of interest as sensing elements in microbolometers. This is particularly the case because of the lack of measurable hysteresis observed through the cooling and heating cycles, and the high conductivity and its rapid rate of change near room temperatures.

ACKNOWLEDGMENTS

The authors acknowledge the support for this work by the UPRM College of Arts and Sciences and partial support by the U.S. Army Research Office under Award No. W911NF-15-1-0448.

[1]F. J. Morin, Phys. Rev. Lett. **3**, 34 (1959).
[2]F. Théobald, R. Cabala, and J. Bernard, J. Solid State Chem. **17**, 431 (1976).
[3]C. Leroux, Ch. Leroux, G. Nihoul, and G. Van Tendeloo, Phys. Rev. B **57**, 5111 (1998).
[4]H. Li, P. He, Y. Wang, E. Hosono, and H. Zhou, J. Mater. Chem. **21**, 10999 (2011).
[5]M. B. Sahana, G. N. Subbanna, and S. A. Shivashankar, J. Appl. Phys. **92**, 6495 (2002).
[6]J.-C. Valmalette and J.-R. Gavarri, Mater. Sci. Eng. B **54**, 168 (1998).
[7]X. J. Wang, H. D. Li, Y. J. Fei, X. Wang, Y. Y. Xiong, Y. X. Nie, and K. A. Feng, Appl. Surf. Sci. **177**, 8 (2001).
[8]A. Chen, B. Zhenxing, W. Zhang, J. Jian, Q. Jia, and H. Wang, Appl. Phys. Lett. **104**, 071909 (2014).
[9]Y. Oka, T. Yao, N. Yamamoto, Y. Ueda, and A. Hayashi, J. Solid State Chem. **105**, 271 (1993).
[10]M. Marezio, D. B. McWhan, J. P. Remeika, and P. D. Dernier, Phys. Rev. B **5**, 2541 (1972).
[11]J. B. Goodenough, J. Solid State Chem. **3**, 490 (1971).
[12]P. A. Cox, *Transition Metal Oxides* (Oxford University Press, New York, 1992).
[13]N. F. Mott, *Metal-Insulator Transitions*, 2nd edition (Taylor and Francis Ltd., London, 1997).
[14]S. Bierman, A. Poteryaev, A. I. Lichtenstein, and A. Georges, Phys. Rev. Lett. **94**, 026404 (2005).
[15]V. Eyert, Phys. Rev. Lett. **107**, 016401 (2011).
[16]S. A. Corr, M. Grossman, Y. Shi, K. R. Heier, G. D. Stucky, and R. Seshadri, J. Mater. Chem. **19**, 4362 (2009).
[17]A. Srivastava, H. Rotella, S. Saha, B. Pal, G. Kalon, S. Mathew, M. Motapothula, M. Dykas, P. Yang, E. Okunishi, D. D. Sarma, and T. Venkatesan, APL Mater. **3**, 026101 (2015).
[18]S. Amoruso, J. Schou, and J. G. Lunney, Appl. Phys. A **92**, 907 (2008).
[19]S. K. Hau, K. H. Wong, P. W. Chan, and C. L. Choy, Appl. Phys. Lett. **66**, 245 (1995).
[20]P. R. Willmott and J. R. Huber, Rev. Mod. Phys. **72**, 315 (2000).
[21]S. Lysenko, V. Vikhnin, F. Fernández, A. Rúa, and H. Liu, Phys. Rev. B **75**, 075109 (2007).
[22]S. Lafane, T. Kerdja, S. Abdelli-Messaci, Y. Khierddine, M. Kechouane, and O. Nemraoui, Appl. Phys. A **112**, 159 (2013).
[23]Powder Diffraction File 81-2392, JCPDS-International Centre for Diffraction Data, PA, USA.
[24]Powder Diffraction File 82-1047, JCPDS-International Centre for Diffraction Data, PA, USA.
[25]W. D. Kingery, H. K. Bowen, and D. R. Uhlmann, *Introduction to Ceramics*, 2nd ed. (John Wiley and Sons, New York, 1976), p. 595.
[26]D. Kucharczyk and Z. Niklewski, J. Appl. Cryst. **12**, 370 (1979).
[27]C. V. Thompson, Annu. Rev. Mater. Res. **20**, 245 (1990).
[28]J. M. Bennett and L. Mattsson, *Introduction to Surface Roughness and Scattering*, 2nd ed. (Optical Society of America, Washington, D.C., 1999).
[29]E. L. Church, P. Z. Takacs, and T. A. Leonard, Proc. SPIE **1165**, 136 (1990).
[30]P.-G. de Gennes, F. Brochard-Wyart, and D. Quèrè, *Capillarity and Wetting Phenomena* (Springer, NY, 2004).
[31]R. Cabriolu and P. Ballone, Phys. Rev. B **81**, 155432 (2010).
[32]J. J. Gilman, J. Appl. Phys. **31**, 2208 (1960).
[33]E. Uchaker, Doctoral dissertation, University of Washington, WA (2015).
[34]L. B. Freund and S. Suresh, *Thin Film Materials: Stress, Defect Formation and Surface Evolution* (Cambridge University Press, Cambridge, 2003), p. 15 et seq.
[35]C. V. Thompson, Annu. Rev. Mater. Res. **42**, 399 (2012).
[36]J. A. Venables, *Introduction to Surface and Thin Film Processes* (Cambridge University Press, Cambridge, 2000).
[37]S. K. Sahu, P. S. Maram, and A. Navrotsky, J. Am. Ceram. Soc. **96**, 3670 (2013).
[38]J. W. Seto, J. Appl. Phys. **46**, 5247 (1975).
[39]N. F. Mott and E. A. Davis, *Electronic Processes in Non-Crystalline Materials*, 2nd ed. (Oxford University Press, Oxford, 1979).
[40]D. Lemoine and J. Mendolia, Phys. Lett. A **82**, 418 (1981).
[41]D. K. Paul and S. S. Mitra, Phys. Rev. Lett. **31**, 1000 (1973).